Tracking accuracy and stability of a sliding peak-filter based controller for spiral nanopositioning in probe storage systems

Andreas Kotsopoulos and Theodore Antonakopoulos

Abstract— High precision nanopositioning is a crucial function of high-density probe-based storage devices and its performance affects determinatively the device's reliability. The use of non-conventional nanopositioning schemes for achieving much higher data rates imposes new requirements on the control algorithms. In this work we analyze in terms of accuracy and stability an H_2 controller combined with a sliding peak-filter for moving along an archimedean spiral trajectory. As it is demonstrated, proper selection of the peak-filter parameters results to a stable and accurately controlled system that achieves high positioning velocities and also supports different read and write data rates.

I. INTRODUCTION

Nanometer-precise positioning at high velocities is a major challenge for rapidly emerging applications that use scanning probes in order to observe and alter the properties of materials down to the nanoscale. Typical examples include surface imaging, nanolithography and data storage [1], [2], [3]. Although data storage technology has demonstrated impressive progress in terms of storage density and reliability, along with remarkable cost reduction per Mbyte, new developments in computing, consumer products and business activities demand storage devices with increased storage capacity and I/O performance.

Near-term technological improvements result to higher areal densities, while more complex and novel recording techniques are investigated that differ radically from those of the present days [5]. One of these technologies, which results to ultrahigh storage densities, is based on the thermo-mechanical scanning-probe-based data-storage approach to write, read back, and erase data in very thin polymer films [7]. High data rates are achieved by using two dimensional arrays of probes operating in parallel. As it has been demonstrated experimentally, high precision positioning on the storage medium is achieved by micro-electromechanical system (MEMS)-based x and y actuators, while the achievement of ultrahigh storage densities is mainly determined by the nanoscale positioning and read-back signal processing for reliable detection [6], [4]. Depending on the application, the storage devices have very strict requirements on the bit-error rate experienced by the user, which is determined by the raw bit-error rate at the read channel and the error control codes used at the system level. The raw bit-error rate of probe-based storage devices is a non-linear function of the nanopositiong error, i.e. the distance of the read-back sensor from the track center line.

The authors are with the Department of Electrical and Computers Engineering, University of Patras, 26500 Rio - Patras, Greece. `akotsop`, `antonako@upatras.gr`

Up to now, probe-based data storage systems have been based on constant linear velocity along a raster-like scan trajectory. Recently, we proposed an alternative nanopositioning scheme that is based on moving along an archimedean spiral trajectory with constant linear velocity, hence maintaining the same positioning resolution throughout the entire trajectory and achieving continuous system operation [8]. In archimedean spiral nanopositioning, motion starts from an initial point away from the medium center and follows a spiral trajectory of equidistant turnings around the center with respect to the medium x/y-plane, until a final radius is reached.

Unlike raster positioning, spiral positioning results in a variable scan frequency when moving along the trajectory with constant linear velocity. The proposed scheme can be used in typical applications, where read and write operations are performed at the same velocity (resulting to the same data rate), or in more demanding applications, like archival storage, where much higher data rates have to be supported when information is retrieved from the storage medium.

In this work, we study the performance of an H_2 controller for spiral nanopositioning that is based on the sliding peak-filter approach. A similar controller has been presented in [10], but for a completely different system and without considering any stability or mixed accuracy/stability issues. Section II highlights the characteristics of the system and presents the modeling procedure, while Section III presents in depth the controller's architecture. Finally, Section IV investigates extensively the controller's accuracy and stability and demonstrates its superior performance compared to a controller that does not employ peak-filters.

II. SYSTEM DESCRIPTION AND MODELING

The control mechanism presented in this work was developed for a model of a scanning-probe data storage experimental setup with thermomechanical and optical read and thermomechanical write capabilities. Information is stored as sequences of indentations written on thin polymer films using an AFM cantilever. Thermomechanical writing is performed by applying an electrostatic force to the polymer layer and simultaneously softening the polymer layer by local heating. Readback is achieved by measuring the thermal conductance between the probe and the storage substrate or the deflection of a laser beam due to the cantilever's displacement. The presence or the absence of indentations corresponds to logical 1s or 0s, respectively.

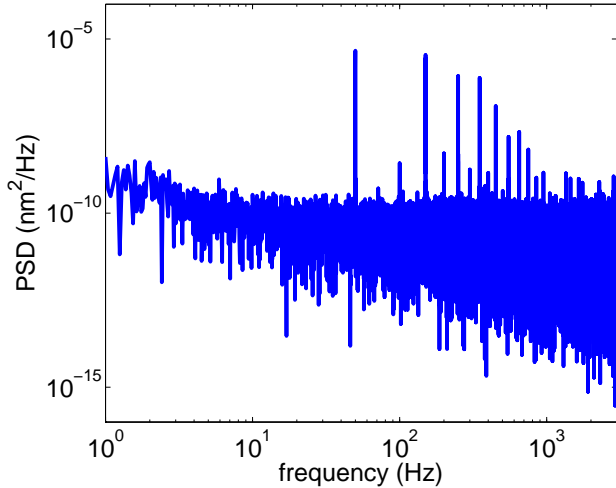The nanopositioning system under consideration is based

Fig. 1. Measured capacitive sensor noise power spectral density.

(a) x-axis

(b) y-axis

Fig. 2. Experimentally obtained frequency response of the scanner in the x and y axes using the integrated capacitive position sensors.

on a piezoelectrically actuated scanner [9], capable of displacing the storage medium with respect to the cantilever tip in the x, y and z axis. The respective travel ranges are 100 μm, 100 μm and 20 μm respectively. Position feedback in the x/y plane is provided by two high-precision capacitive sensors one for each direction of motion and two 18-bit Analog-to-Digital Converters (ADCs). The standard deviation of the combined measurement and quantization noise is 1.51 nm for the x-axis and 1.75 nm for the y-axis, while the overall position resolution in the x and y direction over a range of 10 kHz was found to be 0.96 nm and 1.21 nm, respectively. The measured power spectral density (PSD) of the combined noise is presented in Fig. 1 for the x-axis sensor, showing the relatively high spectral components at the odd multiples of 50 Hz due to ambient electrical noise mainly picked up by the circuitry connecting the sensors with the acquisition board. In a battery powered system, these high spectral components would not be present and they will not disturb the positioning mechanism.
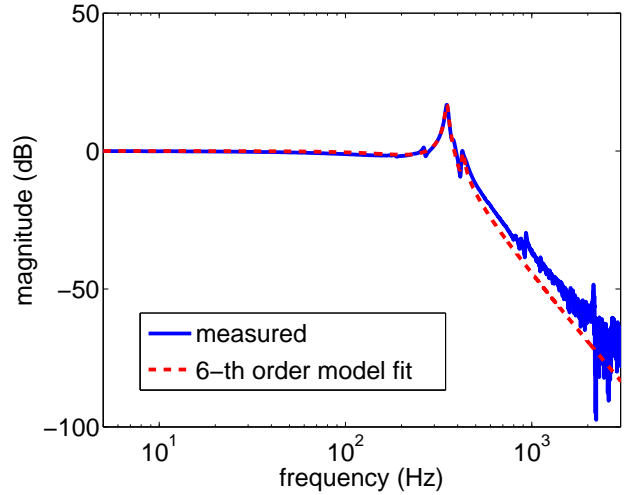
The experimentally obtained frequency responses of the system using the capacitive sensors are depicted in Fig. 2, together with their corresponding sixth-order transfer function fits. The reduced models capture well the first two resonances of the plant and were used for the H_2 controller synthesis process, while the simulations were carried out with a higher order model. The scanner presents an almost flat response until the first resonances, which appear at 374 Hz and 350 Hz in the x and y axis respectively. However, the delays introduced by the high charge/discharge time constants of the capacitive elements (due to the supported long travel ranges), as well as by the external high voltage drive, result in a rather high amount of phase loss. This fact is expected to further limit the bandwidth of the final closed-loop system.

III. THE CONTROLLER ARCHITECTURE

Two individual controllers with identical architecture where used for the control of the nanopositioner, one for
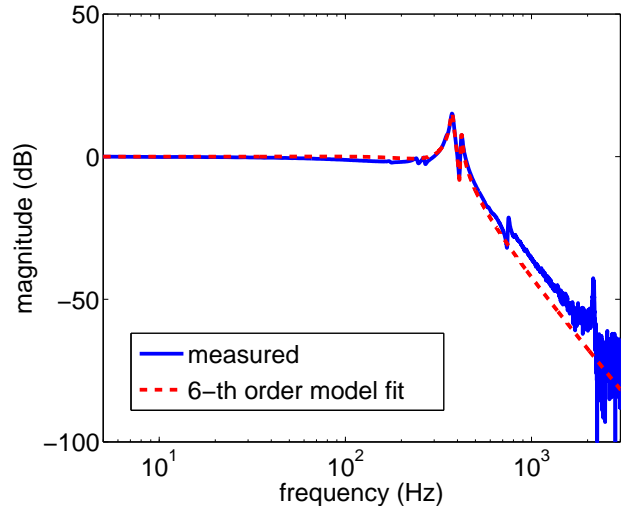
each axis of motion. The control architecture is depicted in the block diagram of Fig. 3. Note that the analysis that follows is presented for the x-axis case only, but holds as is for the y-axis case with similar results. The loop comprises a frequency-sliding peak filter, an H_2 controller denoted by K_{H_2}, and a notch filter denoted by K_{NF}, all connected in a cascade manner.

The H_2 problem formulation is shown in Fig. 4. The sixth-order transfer function fits produced eighth-order controllers in both axes. The shaping specifications for the closed loop transfer functions were captured by the weighting functions W_s and W_u shown in Fig. 5, expressing the requirements on tracking performance and control effort limits respectively. Finally, v and u denote the input to the controller and the controlled output respectively, while $w = [w_1]$ the "exogenous input" signal vector and $z = \begin{bmatrix} z_1 \\ z_2 \end{bmatrix}$ the "exogenous output" signal vectors [12]. The system can then be described
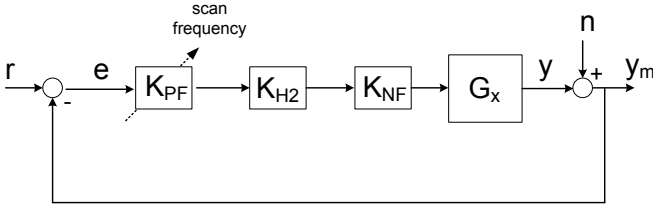
Fig. 3. Block diagram of the one-degree-of-freedom linear time-varying control architecture.
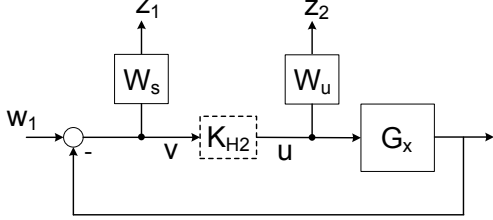

Fig. 4. H_2 control design problem formulation.

Fig. 5. Performance and control input weighting transfer functions.
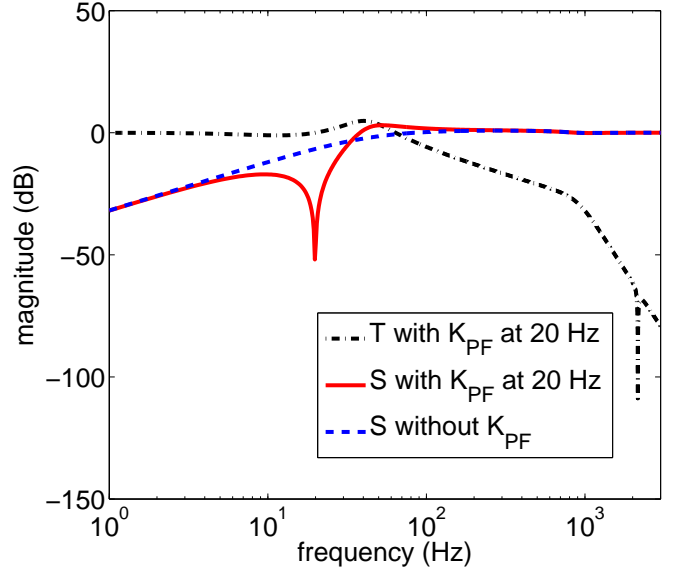
Fig. 6. Closed loop transfer functions for the x-axis.

as:

$$\left[\begin{array}{c} z_1 \\ z_2 \\ v \end{array}\right] = P \cdot \left[\begin{array}{c} w_1 \\ u \end{array}\right], \qquad u = K_{H_2}v \qquad (1)$$

where P denotes the generalized plant given by:

$$P = \left[\begin{array}{cc} W_s & -W_sG_x \\ 0 & W_u \\ 1 & -G_x \end{array}\right] \qquad (2)$$

The closed loop transfer function matrix T_{zw} relating z with w is the linear fractional transformation of K_{H_2} around P, given by:

$$T_{zw} = F_l(P,K) = \left[\begin{array}{c} \frac{W_s}{1+G_xK_{H_2}} \\ \frac{W_uK_{H_2}}{1+G_xK_{H_2}} \end{array}\right] \qquad (3)$$

The peak filter can be constructed according to:

$$K_{PF}(s) = \frac{s^2 + 2\zeta_1\omega_p s + \omega_p^2}{s^2 + 2\zeta_2\omega_p s + \omega_p^2} \qquad (4)$$

where $f_p = \omega_p/(2\pi)$ the instantaneous center scan frequency, and ζ_1,ζ_2 the damping ratios of the filter. The latter can be expressed in terms of the parameters M, N, Δ, where M denotes the magnitude at f_p, and N the magnitude at the frequency points around the center frequency, which are determined by Δ [11]. The parameters are set individually, according to the desired magnitude response of the filter. Finally, in order to compensate for the unmodeled higher order resonances at approximately 2.1 kHz, a notch filter denoted by K_{NF} was used.

The resulting x-axis sensitivity (denoted by S) transfer function, relating the reference input with the tracking error signal, and complementary sensitivity (denoted by T) transfer function, relating the reference with the output, are depicted in Fig. 6. For the cases where the peak filter is
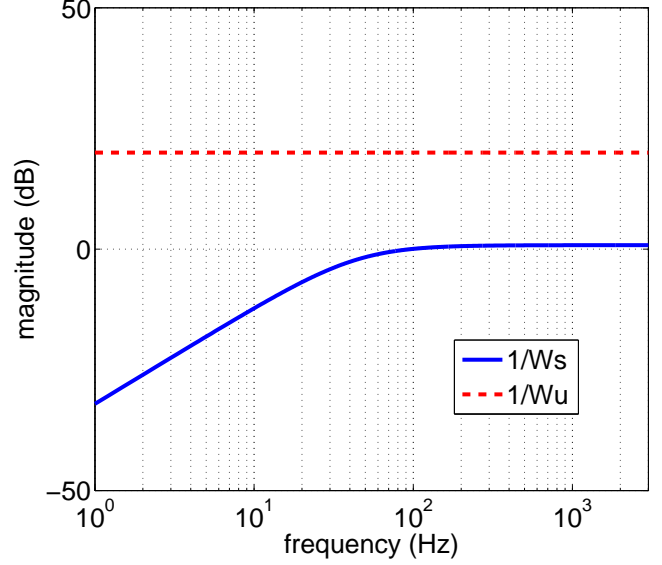
included in the loop, the transfer functions of Fig. 6 represent only time-snapshots of T and S. The controller bandwidth (without the peak filter) was approximately 40 Hz in both axes. In closed form the transfer functions of the combined architecture can readily be calculated as:

$$T = \frac{K_{PF}K_{H_2}K_{NF}G_x}{1 + K_{PF}K_{H_2}K_{NF}G_x} \qquad (5)$$

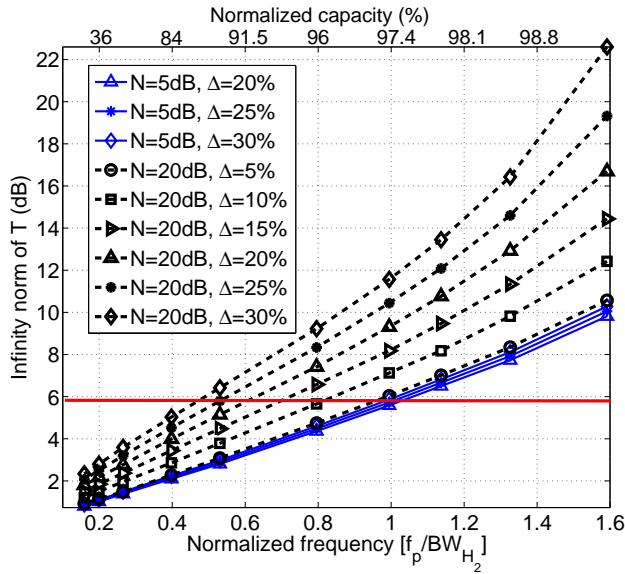$$S = \frac{1}{1 + K_{PF}K_{H_2}K_{NF}G_x} \qquad (6)$$

Fig. 7. Dependance of the infinity norm of the complementary sensitivity transfer function ($\|T\|_\infty$) on the instantaneous scan frequency and the peak filter design parameters N and Δ for M fixed at 140 dB.

Fig. 9. Mean positioning error (Euclidean distance position error) with respect to the scan frequency and the peak filter design parameters N and Δ for M fixed at 140 dB.

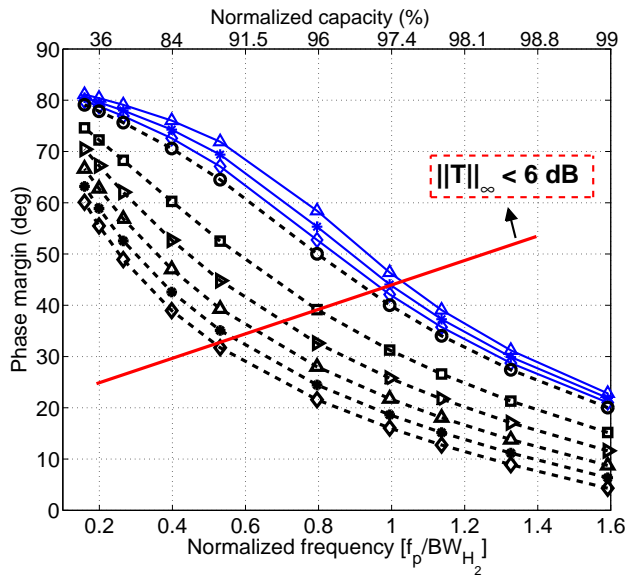
Fig. 8. Dependance of the open loop system's phase margin on the instantaneous scan frequency and the peak filter design parameters N and Δ for M fixed at 140 dB. [Marker and line annotation matches Fig. 7]

Fig. 10. Standard deviation of the positioning error (Euclidean distance position error) with respect to the scan frequency and the peak filter design parameters N and Δ for M fixed at 140 dB.

IV. ACCURACY AND STABILITY ANALYSIS

The bulges in both T and S of Fig. 6 are clearly due to the distortion introduced by the peak filter, pushing the infinity norm of both transfer functions to higher values and reduces the system stability margins. The amount of distortion depends on the selection of the filter parameters M, N, Δ, since they determine the total amount by which the area under the respective transfer function is reduced due to the peak filter insertion. It is well known, that this reduction will be compensated for in some other frequency region of the transfer function causing it to bulge [12]. Moreover,
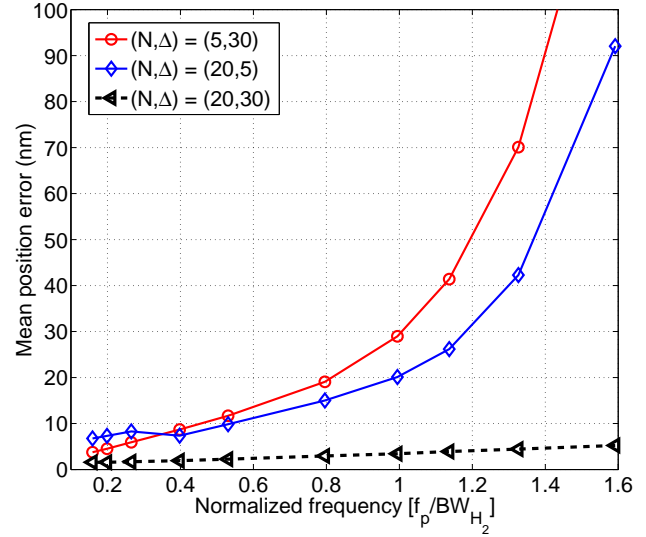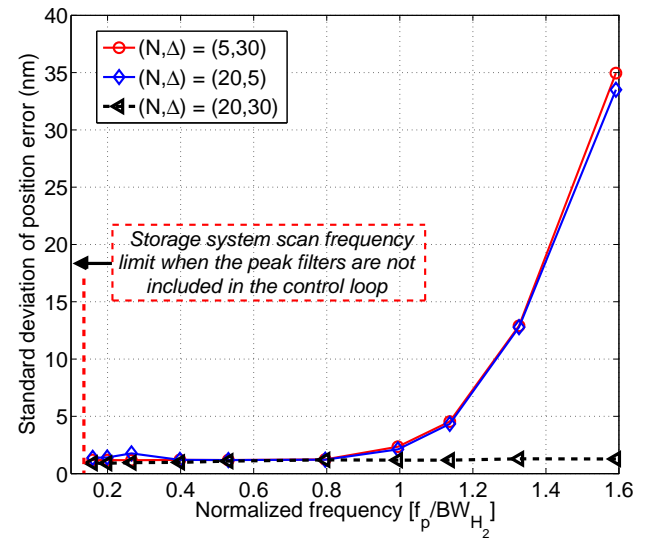
M, N, Δ also vastly determine the tracking capabilities of the loop. Therefore, the final parameter selection results in a trade off between the achieved stability margins and tracking performance.

Note, that for values of M ranging from 40 dB to 140 dB, the effect of M on the stability margins for a fixed value pair of (N, Δ) was found to be negligible. Contrariwise, the margins are dominated by the values of N and Δ. This low dependence on M is reasonable, considering the rather small area covered by the narrow filter part that M shapes. Therefore, M is considered fixed at 140 dB without loss of generality. A high value for M is preferred, since a high

drop of S is required for high positioning accuracy.

Fig. 7 and Fig. 8 show the way the stability margins of the system vary with respect to different combinations of N, Δ, in terms of the $\|T\|_\infty$ and the phase margin, respectively. The scan frequency is normalized with respect to the bandwidth of the H_2 controller presented in Section III. The scan frequency values can be mapped to radii or velocities interchangeably. For example, for a fixed constant linear velocity of 2 nm/μs, the normalized frequency values depicted in the two figures correspond to a 5 - 50 μm radius range. Conversely, for a fixed radius, the values correspond to a constant linear velocity range. It is clear from both figures that as the point of operation moves to scan frequencies beyond the controller bandwidth, the system's stability margins are reduced.

Additionally, in the same figures, the normalized capacity axis shows the achieved capacity ratio with respect to the maximum spiral capacity, if specific stability margin specifications are set (which translate to a minimum supported radius given the constant linear velocity). Notice that a stability requirement corresponding to a minimum allowable radius of half the maximum radius, results in a less than 10% capacity loss. This is due to the capacity being a quadratic function of the spiral radius.

In Fig. 9 and Fig. 10 comparative simulation results are depicted, showing the effect of the filter parameters N, Δ on the achieved positioning precision. The performance metric used is the mean and standard deviation of the euclidean distance between the reference spiral points and the reached points on the x/y plane.

Considering the joint requirements for robustness against noise and unmodeled dynamics and positioning accuracy in probe storage systems, the results presented in Fig. 7 - 10 have to be evaluated in parallel. Two distinct cases can be distinguished: firstly, when all positioning operations are performed at the same constant linear velocity, and secondly, when different velocities have to be supported. In the first case, the mean error value is not decreasing the performance limits of the system, since the same position offset is introduced in every system operation (read, write, erase) and can therefore be ignored or compensated for using feed-forward action. Consequently, lower values for N, Δ can be selected, resulting in both positioning accuracy below 5 nm at high velocities and better stability margins. In the second case, the trade off between the two requirements cannot be avoided.

Finally, it should be mentioned that the closed loop system under investigation is essentially a linear time-varying (LTV) system. It is well known from the literature [13], that frozen-time stability does not imply stability of the LTV system. Although the properties of the system considered here are such that it can be categorized to the special class of slowly varying systems [14], a formal mathematical proof falls outside the scope of this work, and is part of ongoing work.

Nevertheless, at least in the context of simulations, the rate of variation of the system parameters, namely of the center frequency of the peak filter, does not seem to lead the system to instability.

V. CONCLUSIONS

The performance of an H_2 controller combined with frequency sliding peak filters for spiral nanopositioning, in terms of stability and positioning accuracy, has been investigated in detail. The way to select the filter's parameters based on the prospective system specifications (stability margins, accuracy, single/multiple data rates) has been also presented thoroughly.

Simulation results demonstrated that the controller achieves good frozen-time stability margins and positioning precision that satisfy the strict requirements posed by applications like ultra-high-density probe storage at scan frequencies near the controller bandwidth. Compared to a stand-alone H_2 controller of the same bandwidth, the increase in supported scan velocity, given the accuracy specifications, is remarkable. Finally, ongoing and future work includes a formal analytical stability investigation of such time-varying systems and corroboration with experimental results.

VI. ACKNOWLEDGMENTS

REFERENCES

[1] B. Bhushan, *Handbook of Nanotechnology*, 2004, Springer Verlag, Germany.
[2] M. Shibata, H. Yamashita, T. Uchihashi, H. Kandori, and T. Ando, "High-speed atomic force microscopy shows dynamic molecular processes in photoactivated bacteriorhodopsin", *Nature Nanotechnology*, 5, pp. 208-212.
[3] S. Mishra, J. Coaplen, and M. Tomizuka, "Precision positioning of wafer scanners", *IEEE Control Systems Magazine*, 27(4), pp. 2025.
[4] A. Sebastian, A. Pantazi, H. Pozidis, E. Eleftheriou, "Nanopositioning for probe-based data storage, *IEEE Control Systems Magazine*, 2008.
[5] P. H. Siegel, E. Soljanin, et al. (Edts), "Advances in Information Recording", DIMACS Series, Vol. 73, Americam Mathematical Society, 2004.
[6] A. Pantazi, A. Sebastian, et al., "Probe-based ultrahigh-density storage technology", *IBM Journal of Research and Development*, Vol. 52, No. 4/5, July/September 2008.
[7] H. Pozidis, W. Haberle, D. Wiesmann, U. Drechsler, M. Despont, T. R. Albrecht, and E. Eleftheriou, "Demonstration of Thermomechanical Recording at 641 Gbit/in2", *IEEE Transactions on Magnetics*, Vol. 40, No. 4, July 2004, pp. 2531-2536.
[8] A. Kotsopoulos and T. Antonakopoulos, "Nanopositioning using the spiral of archimedes: The probe-based storage case", *Mechatronics*, 20(2), 2010.
[9] S. Devasia, E. Eleftheriou, and S.O.R. Moheimani, "A survey of control issues in nanopositioning", *IEEE Trans. on Control System Technology*, 15(5), 2007.
[10] A. Kotsopoulos, A. Pantazi, and T. Antonakopoulos, "Control for high speed archimedean spiral nanopositioning", *The 17th IEEE International Conference on Electronics, Circuits, and Systems, ICECS*, December 2010, Athens, Greece.
[11] A.A. Mamun, G. Guo, and C. Bi, "Hard Disk Drive Mechatronics and Control", 2007, CRC Press.

[12] S. Skogestad and I. Postlethwaite, "Multivariable feedback control: analysis and design", 2005, Wiley-Interscience, 2nd edition.

[13] Wilson J. Rugh, "Linear system theory", 2nd edition, Prentice Hall, 1996.

[14] C. A. Desoer, "Slowly Varying System $\dot{x} = A(t)x$", *IEEE Transactions on Automatic Control*, December, 1969.